ACS APPLIED MATERIALS & INTERFACES

Research Article

www.acsami.org

In Situ Transmission Electron Microscopy Observation of the Lithiation–Delithiation Conversion Behavior of CuO/Graphene Anode

Qingmei Su,[†] Libing Yao,[†] Jun Zhang,[†] Gaohui Du,[*,†,‡] and Bingshe Xu[‡]

[†]Institute of Physical Chemistry, Zhejiang Normal University, Jinhua 321004, China

[‡]Research Centre of Advanced Materials Science and Technology, Taiyuan University of Technology, Taiyuan, 030024 Shanxi, China

Supporting Information

ABSTRACT: The electrochemical conversion behavior of metal oxides as well as its influence on the lithium-storage performance remains unclear. In this paper, we studied the dynamic electrochemical conversion process of CuO/graphene as anode by in situ transmission electron microscopy. The microscopic conversion behavior of the electrode was further correlated with its macroscopic lithium-storage properties. During the first lithiation, the porous CuO nanoparticles transformed to numerous Cu nanograins (2–3 nm) embedded in Li_2O matrix. The porous spaces were found to be favorable for accommodating the volume expansion during lithium insertion. Two types of irreversible processes were revealed during the lithiation–delithiation cycles. First, the nature of the charge–discharge process of CuO anode is a reversible phase conversion between Cu_2O and Cu nanograins. The delithiation reaction cannot recover the electrode to its pristine structure (CuO), which is responsible for about ~55% of the capacity fading in the first cycle. Second, there is a severe nanograin aggregation during the initial conversion cycles, which leads to low Coulombic efficiency. This finding could also account for the electrochemical behaviors of other transition metal oxide anodes that operate with similar electrochemical conversion mechanism.

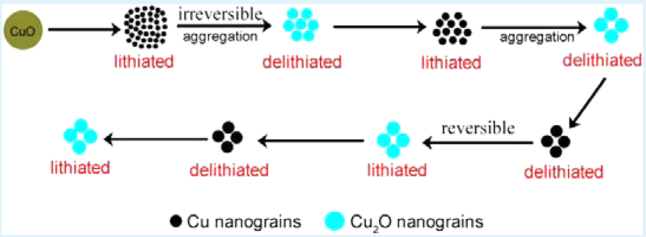

KEYWORDS: *transmission electron microscopy, metal oxide, conversion mechanism, lithium-ion battery, nanograin aggregation*

1. INTRODUCTION

Rechargeable lithium-ion batteries (LIBs) are now considered as a preferred energy storage system for electric vehicles and portable electronic devices.[1,2] The growing demand for energy has greatly excited recent research on developing high-performance electrode materials with enhanced safety, great power densities, and high rate performance along with a substantial increase in cycle life.[3] Therefore, there has been an immense increase in research on new electrode materials with promising electrochemical capacity for use in LIBs.[1] Currently, great efforts have made to investigate transition metal oxides as anode materials for LIBs due to their large theoretical capacity (500–1000 mAh g^{-1}). However, the application of metal oxides as anode in LIBs is still severely impeded by their low conductivity and poor cycling stability.[4,5] One effective way to mitigate these problems is to fabricate special nanostructures with short Li-ion diffusion distance and high surface area. Substantial efforts have been dedicated to the facile synthesis of new electrode materials with special design such as one-dimensional (1D) micro/nanostructures,[6,7] porous structures,[8,9] hollow structures,[10,11] and multishelled structures.[12,13] In particular, porous micro/nanostructures materials have attracted great interest owing to their advantageous features for facile Li^+ ion insertion and small capacity fading.

CuO has attracted particular interest as one of the promising metal oxide anode materials to replace the conventional carbon anodes (with theoretical capacity of 372 mAh g^{-1}) due to high theoretical capacity (670 mAh g^{-1}),[14] low cost, and eco-friendliness.[15] Moreover, nanosized transition metal oxides undergo a conversion reaction in LIBs according to the equation proposed by Poizot et al.,[16] $M_aO_b + (2b)Li \leftrightarrow aM + bLi_2O$, where M is transition metal such as Fe, Ni, Co, Cu, etc. The electrochemical conversion reaction of CuO nanowires has been preliminarily investigated by Wang et al.[17] Recently, many kinds of CuO/graphene composites have been prepared and showed greatly improved lithium-storage performance.[15] It is urgent to reveal the conversion behaviors of CuO nanoparticles anchored graphene sheets during charge–discharge cycles. In general, there is a large capacity loss for metal oxide anodes in the initial electrochemical cycles, and the capacity fading is mainly interpreted in terms of irreversible electrochemical processes. So far, the nature of the irreversible electrochemical process of CuO anode is still not well understood.[2,18] In other words, how the nanostructures evolve within the CuO anode

Received: July 19, 2015
Accepted: October 6, 2015
Published: October 6, 2015

DOI: 10.1021/acsami.5b06548
ACS Appl. Mater. Interfaces 2015, 7, 23062–23068

and further influence its lithium-storage performance remains unclear.

Direct observation of the dynamic lithiation−delithiation behavior of anodes has been achieved using in situ transmission electron microscopy (TEM) studies.[19−22] The visualization of the conversion process can reveal the reaction mechanism of electrode materials and thus facilitate the design of high-performance materials for LIBs.[23−26] In this paper, we fabricated a nanoscale LIB inside a high-resolution TEM using an individual porous CuO/graphene as electrode and directly observed its microstructure evolution in lithiation−delithiation cycles. The microscopic electrochemical behavior and conversion mechanisms of porous CuO nanoparticles have been revealed and further correlated with its macroscopic electrochemical lithium-storage performance.

2. EXPERIMENTAL SECTION

2.1. Preparation of CuO/Graphene. Graphite oxide (GO) was prepared from graphite flakes using a modified Hummers' method.[27] To prepare porous CuO/graphene, GO (0.12 g) was dispersed in 80 mL of ethanol with sonication for 30 min to achieve a homogeneous dispersion. Then 0.66 g of $Cu(Ac)_2{\cdot}H_2O$ was dissolved in the above solution, and 8 mL of $NH_3{\cdot}H_2O$ (10 M) was dropped into the above solution. The mixture was placed in a microwave oven and heated for 10 min with the microwave power of 500 W. GO nanosheets were reduced during the microwave-heating process. Finally, the obtained gray products (CuO/graphene) were collected for the in situ TEM study and electrochemical tests.

2.2. In Situ TEM Experiments. The in situ lithiation−delithiation experiments were conducted inside a TEM (JEM-2100F) with a TEM−STM holder (Nanofactory). Briefly, the all-solid nanosized electrochemical device consists of three essential components: an individual CuO/graphene nanosheet as the working electrode, a Li particle as the counter electrode, and a layer of Li_2O grown on Li particle as the solid electrolyte. The detailed preparation procedure for the nano-LIB can be found in literature.[22] During the in situ experiments, the potentials of −1 V were applied to CuO/graphene electrode with respect to the Li electrode to drive lithiation (Li^+ insertion), and the bias was reset to +3 V to realize the delithiation of CuO electrode. Electron beam irradiation effect was eliminated in the in situ TEM experiments by blocking the electron beam except for short time imaging.

2.3. Electrochemical Performance Measurement. The electrochemical lithium-storage performance of CuO/graphene was tested with a two-electrode 2032-type coin cell using pure Li foil (Aldrich) as the counter electrode. The working electrodes were prepared by spreading the slurry of CuO/graphene, polyvinylidene fluoride (PVDF), and acetylene black in a weight ratio of 75:10:15 in N-methyl pyrrolidone onto Ni foam current collectors. The electrolyte was 1.0 M $LiPF_6$ dissolved in a mixture of dimethyl carbonate and ethylene carbonate (1:1 volume ratio). Galvanostatic charge/discharge cycle was tested between 0.01 and 3 V on a Neware battery cycler at 50 mA g^{-1}.

3. RESULTS AND DISCUSSION

Figure 1, panel a is a TEM image of the as-prepared CuO/graphene composite, revealing that many porous CuO nanoparticles of 60−120 nm are uniformly dispersed on graphene sheets. Further insight into the morphology and microstructure of individual CuO nanoparticles was clarified by a high-magnification TEM image shown in Figure 1, panel b. The porous CuO nanoparticle is constructed from many interconnected nanograins with a size of about 5 nm. Figure 1, panel c displays a HRTEM image of a CuO nanoparticle with well resolved fringes. The inset of Figure 1, panel c is the fast Fourier transform (FFT) pattern of a nanograin, which can be

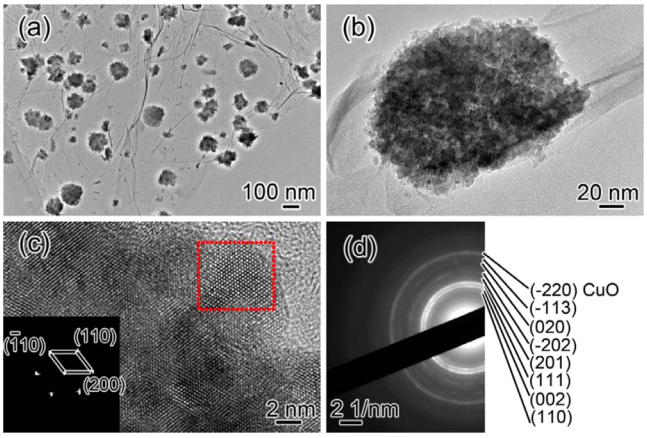

Figure 1. (a) TEM image of porous CuO nanoparticles anchored on graphene nanosheets. (b) High-magnification TEM image of an individual CuO nanoparticle. (c) HRTEM image of a CuO nanoparticle and the FFT pattern (the inset) of the image within the red box. (d) ED pattern of the CuO/graphene.

indexed as the (200), (110), and (−110) planes of the monoclinic structure of CuO (JCPDS card no. 89−5895). The electron diffraction (ED) pattern recorded from the CuO/graphene is displayed in Figure 1, panel d, and it can be well indexed as the monoclinic CuO (JCPDS card no. 89−5895). Both TEM and ED analyses indicate the obtained products are CuO/graphene composites with porous CuO nanoparticles anchored on graphene nanosheets uniformly.

The in situ nanoscale LIB setup for TEM study is illustrated in Figure 2, panel a, which consists of CuO/graphene electrode, Li counter electrode, and Li_2O solid electrolyte. Figure 2, panel b is a TEM image of the pristine CuO/graphene electrode. The initial size of the three CuO nanoparticles anchored on graphene was 103, 87, and 67 nm, respectively. After the CuO electrode was lithiated by applying −1 V potential to the CuO/graphene, the sizes of the three CuO nanoparticles increased to 118, 99, and 78 nm as shown in Figure 2, panel c. The volumetric expansion of these particles is calculated to be 50.4%, 47.3%, and 57.8% based on their size increases. Movies S1 and S2 are provided in the Supporting Information to present the dynamic lithiation reaction of individual CuO nanoparticles on graphene nanosheets. Figure 2, panels d and e show the evolution of two CuO nanoparticles during the lithiation. The microstructures of the CuO nanoparticles changed gradually from one side to another during the lithiation process along the Li^+ diffusion direction. The lithiation of CuO nanoparticle in Figure 2, panel d was completed in 32 s, and the diameter expanded from 163 to 189 nm after lithiation, corresponding to a lithiation ratio of about 0.81 nm/s. However, the second CuO nanoparticle in Figure 2, panel e expanded its size from 114 to 133 nm within 16.5 s after lithiation with a lithiation ratio of about 1.15 nm/s. The difference in lithiation rate can be relevant with the particle size and the local Li^+ concentration around the particles. Furthermore, we checked the other ten CuO nanoparticles, and their volume expansion varied from 47.2−58.8%; the mean volumetric expansion was found to be 52.6%, which is much smaller than the theoretical volumetric expansion of CuO (~82%).[28] The experimentally smaller volume expansion can be contributed to the porous structure of CuO nanoparticles. The porous space can accommodate the volume change during lithium insertion reaction, which is beneficial for the stability of

DOI: 10.1021/acsami.5b06548
ACS Appl. Mater. Interfaces 2015, 7, 23062−23068

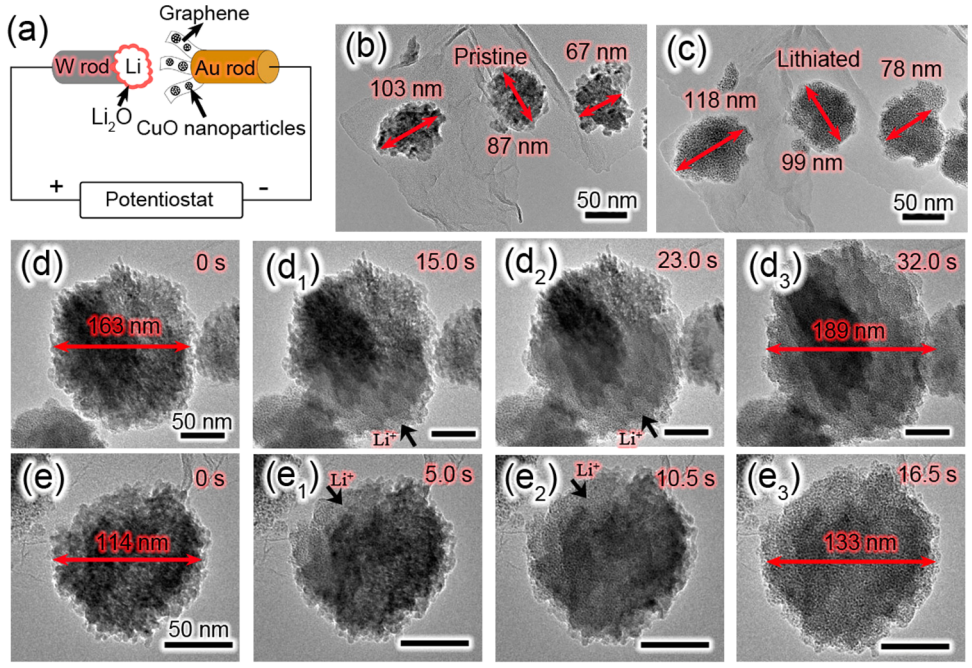

Figure 2. (a) Illustration of the electrochemical setup for in situ TEM. (b) TEM image of the pristine CuO/graphene electrode in a nano-LIB. (c) CuO/graphene electrode after lithiation. (d, e) Evolution of individual CuO nanoparticles over time during lithiation. The scale bars are 50 nm.

electrode and can improve the reversible lithium−storage capacity.

Figure 3 shows the detailed information on the morphology and microstructure of the lithiated CuO nanoparticles. It is

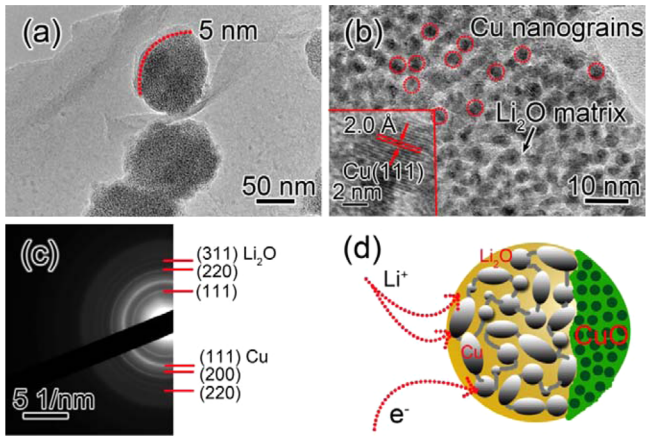

Figure 3. (a) TEM images of CuO/graphene after lithiation. (b) High-magnification TEM image recorded from a lithiated CuO nanoparticle. The red circles indicate the formation of Cu grains. Inset of panel b is a HRTEM image of the Cu nanograins. (c) ED pattern of the lithiated CuO. (d) Schematic illustration of the reaction front in a single CuO particle and the pathway for Li^+ ion and electron transport.

clear that the surfaces and edges of graphene and CuO nanoparticles were coated with thin shells (Figure 3a), which were identified to be Li_2O through ED analysis (Figure 3c). The Li_2O shells are around 2−5 nm in thickness. From the high-magnification TEM image of a lithiated CuO nanoparticle (Figure 3b), it can be found that many Cu nanograins of 2−3 nm were formed in the lithiation process. The HRTEM image of a formed nanograin is given in the inset (Figure 3b), and the fringe spacing of 2.0 Å agrees well with the (111) plane of cubic Cu, which confirms the formation of Cu nanograins in the lithiation process. The dark contrast spots are Cu nanoparticles (marked by red circles), which form a connected network in the Li_2O matrix. The ED pattern recorded from the lithiated CuO particle is displayed in Figure 3, panel c and can be assigned to the mixed phases of Cu and Li_2O (JCPDS no. 77−2144), which suggests that the lithiation reaction involves the conversion of CuO to Cu nanograins along with the formation of Li_2O. The electrochemical reaction can be expressed as $CuO + 2Li^+ + 2e^- \rightarrow Cu + Li_2O$. A schematic illustration of the reaction front in a single CuO nanoparticle is displayed in Figure 3, panel d, which shows the proposed electron and Li^+ ions pathways. The newly formed Cu network can work as an efficient conductive pathway for electron transport into the CuO nanoparticle, while the Li_2O provides a similar pathway for Li^+ ions.

To reveal the conversion mechanism during charge−discharge cycling, the continual lithiation−delithiation processes of an individual CuO nanoparticle in CuO/graphene electrode were recorded by in situ TEM (Figure 4). The pristine CuO nanoparticle of ∼120 nm is located on a few-layer graphene nanosheet (Figure 4a); its ED pattern is shown in Figure 4, panel a_1 and can be well indexed as monoclinic CuO (JCPDS card no. 89−5895). After the first lithiation process, this CuO nanoparticle was inflated and expanded its size to 137 nm with a volume expansion of 47.5%; meanwhile, a thin Li_2O layer appeared on the surface of lithiated CuO nanoparticle as shown in Figure 4, panel b. The ED pattern of the lithiated CuO can be indexed as the mixed phases of Cu and Li_2O (Figure 4b_1), suggesting the electrochemical transformation of CuO to Cu in the first lithiation process. The delithiation process was achieved by resetting the bias of the CuO/graphene electrode to +3 V. Figure 4, panel c shows the TEM image of the delithiated CuO; this single nanoparticle became smaller from 137 to 127 nm in diameter, and the Li_2O layers basically disappeared after the delithiation. The volumetric expansion ratio of the first delithiated nanoparticle to the pristine one is 1.06, indicating an irreversible change in size. As

DOI: 10.1021/acsami.5b06548
ACS Appl. Mater. Interfaces 2015, 7, 23062−23068

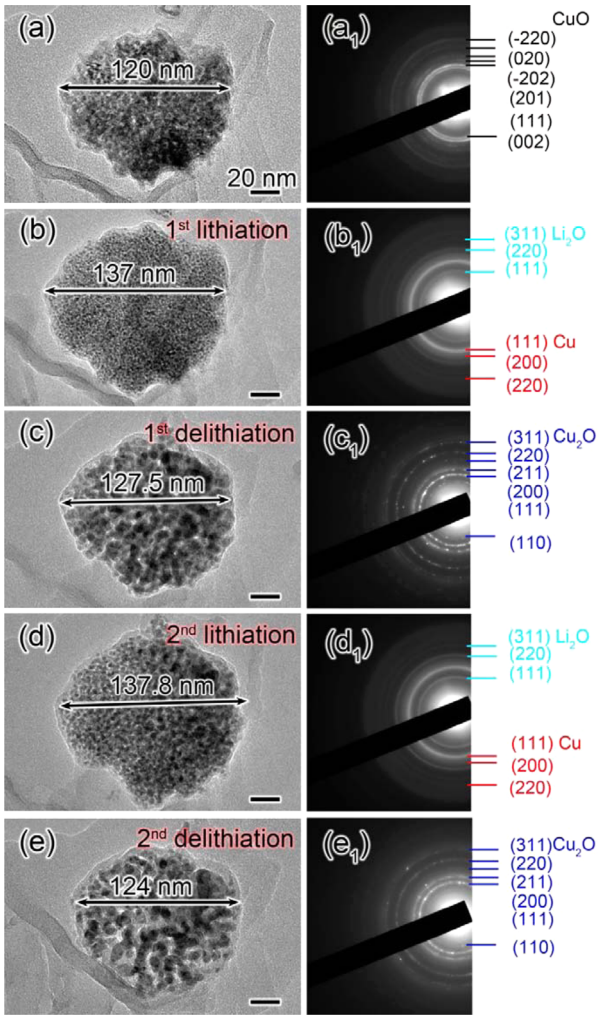

Figure 4. Microstructure evolution of CuO nanoparticle in the electrochemical lithiation and delithiation cycles. (a) The pristine CuO nanoparticle. (b) The first lithiated and (c) delithiated CuO nanoparticle. (d) The second lithiated and (e) delithiated CuO nanoparticle. (a_1–e_1) ED patterns recorded from the corresponding CuO electrode in panels a–e.

shown in Figure 4, panel c_1, the ED pattern of the first delithiated nanoparticle with the appearance of obvious rings corresponds to Cu_2O. It indicates a conversion from Cu into Cu_2O rather than CuO after the first delithiation. This irreversible phase conversion can account for the initial capacity loss because of the reduced theoretical capacity of Cu_2O (375 mAh g^{-1}) as compared to CuO (670 mAh g^{-1}). It suggests the high electrochemical reactivity of Cu nanograins, which enables the decomposition of Li_2O during the delithiation process. The CuO nanoparticles undergo an irreversible phase conversion during the first charge–discharge cycle; in other words, the delithiation process cannot return the electrode to its pristine state (CuO). After the second lithiation process, the size of the observed nanoparticle was 137.8 nm, and the Li_2O layer formed again during the lithiation (Figure 4d). The ED pattern (Figure $4d_1$) confirms that the second lithiated CuO electrode is composed of Cu and Li_2O. The selected CuO nanoparticle shrank its size from 137.8 to 126 nm after the second delithiation as shown in Figure 4, panel e. The ED pattern (Figure $4e_1$) of the second delithiated CuO reveals that the Cu nanograins converted to Cu_2O nanograins during the second delithiation. Compared with the pristine CuO nanoparticle, the total volumetric expansion after the second lithiation and delithiation are 51.4% and 17.1%, respectively. The results indicate that the selected nanoparticle underwent relatively reversible volume changes and phase conversion in the second lithiation–delithiation cycle. The in situ TEM results demonstrate that the first lithiation–delithiation cycle of CuO is irreversible due to the formation of Cu_2O, but the electrochemical conversion between Cu and Cu_2O is reversible during the subsequent cycles, and this process can be expressed as $2Cu + Li_2O \leftrightarrow Cu_2O + 2Li^+ + 2e^-$. The electrochemical conversion of CuO nanoparticles anchored on graphene nanosheets is found to be similar to CuO nanowires.[17] However, we found a new phenomenon about the sizes of Cu nanograins, which increase from ~2.5 nm in the first lithiation (Figure 4b) to ~4 nm in the second lithiation process (Figure 4c).

To quantitatively reveal the nanograin evolution in an individual CuO nanoparticle during the continuous electrochemical cycles, a series of TEM images of a single CuO nanoparticle and the measured nanograin size distribution in the initial four cycles are displayed in Figure 5. A TEM image of the first lithiated CuO is shown in Figure 5, panel a; the Cu nanograin sizes range from 2–3 nm (Figure $5a_1$). During the delithiation process, an abrupt increase in nanograins was observed because Cu nanograins converted to Cu_2O. The TEM image of the delithiated CuO is displayed in Figure 5, panel b; the sizes of Cu_2O nanograins vary from 5–8.4 nm as shown in Figure 5, panel b_1. In theory, the size increase should be about 18% when a single Cu nanograin converts to a single Cu_2O nanograin. The experimental size increase is about 160% for the conversion from Cu to Cu_2O nanograins, indicating a severe aggregation of the nanograins during the electrochemical conversion. In other words, about ten Cu nanograins aggregated and electrochemically converted to a single Cu_2O nanograin during the first delithiation process. After the second lithiation process, the sizes of Cu nanograins are found between 3 and 5 nm as displayed in Figure 5, panel c_1, which is much larger than the Cu nanograins in the first lithiation. Similarly, the sizes of the Cu_2O nanograins are 5–8.4 nm as shown in Figure 5, panel d_1 after the second delithiation. The grain size increase (~71%) observed in the second cycle is much smaller than the increase (160%) in the first cycle but is still larger than the theoretical value (18%), indicating the nanograin aggregation conversion happens also in the second cycle. Therefore, the nanograin size is not reversible even though a reversible phase conversion between Cu and Cu_2O is observed during the second cycle. In the third lithiation–delithiation cycle, the Cu nanograins increase to 4.8–8.2 nm (the mean size is 6.2 nm), and the Cu_2O nanograins are about 5.2–9 nm with a mean size of 7.1 nm. The size change is about 15%, which is quite close to the theoretical value and exhibits a relatively reversible conversion between individual Cu and Cu_2O nanograins. Interestingly, the nanograins in the fourth cycle show a similar size distribution as that in the third cycle, suggesting a stable conversion between Cu and Cu_2O nanograins after the second cycle. It indicates that the CuO electrode undergoes a more reversible microstructural evolution after the second lithiation–delithiation cycle, which is beneficial for a stable electrochemical performance.

Solid electrolyte is used in the in situ TEM experiment, which is different with the typical liquid electrolyte in real LIBs. Also, electron irradiation in TEM is a possible reason for the

DOI: 10.1021/acsami.5b06548
ACS Appl. Mater. Interfaces 2015, 7, 23062–23068

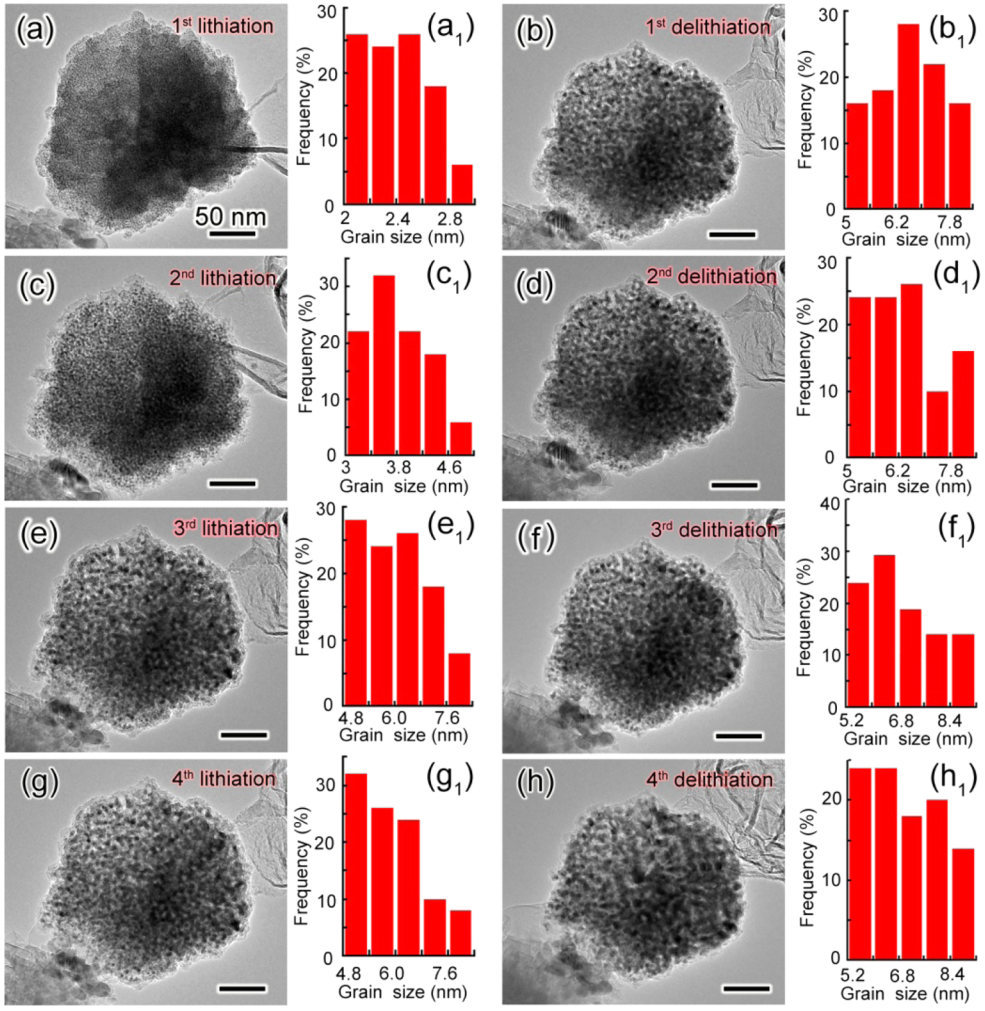

Figure 5. (a–h) Microstructure evolution of a CuO nanoparticle on the electrode during the initial four lithiation and delithiation cycles. (a) The first lithiated and (b) delithiated CuO nanoparticle. (c) The second lithiated and (d) delithiated CuO nanoparticle. (e) The third lithiated and (f) delithiated CuO nanoparticle. (g) The fourth lithiated and (h) delithiated CuO nanoparticle. (a_1–h_1) Histograms of the grain size distribution obtained by counting about 50 nanograins from TEM images in panels a–h.

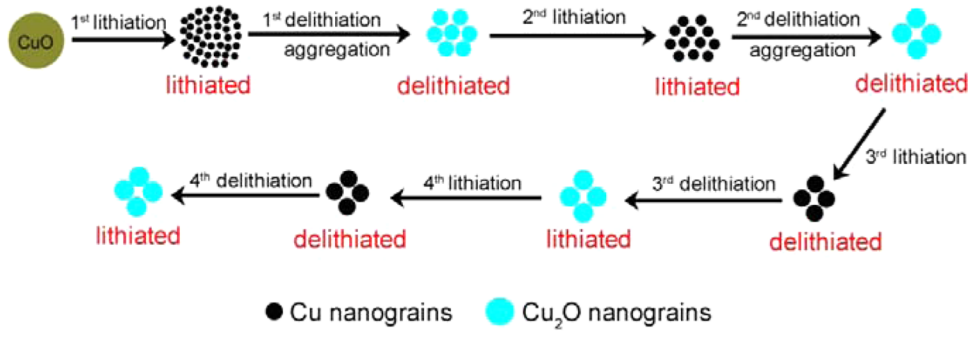

Figure 6. Illustration showing the size change of nanograins within CuO electrode during the four cycles. The li_2O product was omitted for clarity.

nanograin aggregation, though we try to minimize it during the observation. To justify the nanograin aggregation during the electrochemical process, we assembled coin cells using CuO/graphene as the working electrode. After several charge–discharge cycles, the cells were disassembled, and the electrode materials were examined by TEM. The ex situ TEM analysis is shown in Figure S1 in the Supporting Information. Similar nanograin aggregation was observed in the ex situ experiments, which confirms that our in situ TEM results are reliable. Previous papers also presented the similar phenomenon about nanograin aggregation in Si and SnO materials during electrochemical reaction.[29,30] We suggest that the possible driving force for the nanograin aggregation during conversion is the high surface energy of ultrafine nanograins. The numerous nanograins tend to reduce their surface energy by merging of adjacent nanograins during conversion process. Especially when the Li^+ ions bonded with Cu atoms are extracted from the Cu nanograins in the delithiation process, those neighboring Cu

DOI: 10.1021/acsami.5b06548
ACS Appl. Mater. Interfaces 2015, 7, 23062–23068

atoms may show a strong affinity to bond together and result in an aggregated nanoparticle. The nanograin evolution in CuO nanoparticles during the electrochemical cycling is illustrated by Figure 6.

The in situ TEM results were correlated with the macroscopic electrochemical performance of CuO/graphene electrode by assembling coin cells and analyzing the galvanostatic charge−discharge behaviors. The capacity retention of CuO/graphene electrode is presented with the Coulombic efficiency in Figure 7. The CuO/graphene electrode

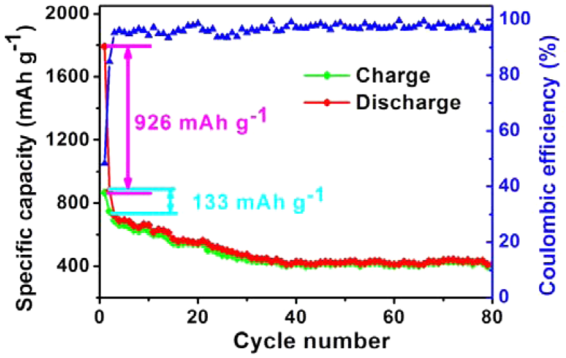

Figure 7. Capacity retention and Coulombic efficiency of CuO/graphene electrode at 50 mA g^{-1}.

is first discharged (lithiation reaction) and showed an initial discharge capacity of 1792 mAh g^{-1}. However, the capacity reduces to 866 mAh g^{-1} in the first charge (delithiation reaction), indicating a capacity loss of 926 mAh g^{-1}. The Coulombic efficiency of CuO/graphene electrode is 48.3% in the first cycle. The TEM investigation on the continual conversion process revealed that there should be a large capacity loss in the initial cycle because the theoretical capacity of Cu_2O is lower than that of CuO. The theoretical capacity loss caused by this irreversible phase conversion is about 295 mAh g^{-1}. It has been reported that the electrode pulverization, irreversible phase changes, and the irreversible formation of SEI membrane are the major factors that lead to large capacity loss for LIBs.[31] To exclude the effect of graphene, we investigated the capacity loss of pure CuO in the first cycle in literature, which is 405 mAh g^{-1} for porous CuO microspheres, 750 mAh g^{-1} for flower-like CuO, 615 mAhg^{-1} for thorn-like CuO,[32] 380 mAhg^{-1} for CuO nanowires,[33] 690 mAh g^{-1} for hollow spherical CuO, and 406 mAh g^{-1} for oatmeal-like CuO.[34] The average initial capacity loss for pure CuO is ∼541 mAh g^{-1}. Our result reveals that around 55% of the initial capacity fading of CuO anodes is caused by the irreversible phase conversion; about 45% of the capacity loss can be resulted from electrode pulverization and other irreversible electrochemical processes. The second discharge and charge processes deliver a capacity of 879.8 and 746.7 mAh g^{-1} with a capacity loss of 133.1 mAh g^{-1}, and the Coulombic efficiency of CuO/graphene electrode is 85% in the second cycle, which is much larger than that in the first cycle due to the reversible phase change between Cu and Cu_2O nanograins. The large capacity fading during the second cycle could be resulted from the severe nanograin aggregation conversion as revealed by the in situ TEM observation, while the conclusion needs further investigation and confirmation. The nanograin sizes tend to be reversible from the third cycles; meanwhile, the Coulombic efficiency increases to ∼94%, which suggests the low Coulombic efficiency in the second cycle is indeed associated with the nanograin aggregation.

4. CONCLUSIONS

We have studied the lithiation−delithiation cycles of porous CuO/graphene electrodes using in situ TEM. The microscopic conversion behaviors of CuO/graphene were further correlated with its lithium-storage performance. Direct observation on the CuO/graphene electrode revealed that the CuO nanoparticles convert to many Cu nanograins coated with Li_2O shells after the first lithiation. The porous spaces are found to be favorable for accommodating the volume change during lithium insertion reaction. The lithiation−delithiation cycles are found to be different from the general conversion mechanism and show two types of irreversible processes. First, the nature of charge−discharge process of CuO anode is a reversible phase conversion between Cu_2O and Cu nanograins. The delithiation process cannot recover the system to the original one (CuO), which is responsible for about 55% of the capacity fading in the first cycle. Second, there is a severe nanograin aggregation during the initial conversion cycles, which leads to low Coulombic efficiency. The nanograin sizes begin to stabilize in the third cycle, corresponding to an enhanced Coulombic efficiency up to ∼94%. Therefore, the nanograin size variation strongly influences the lithium-storage performance and Coulombic efficiency. This finding about the irreversible processes in CuO electrode could be extended to other transition metal oxide anodes that operate with similar electrochemical conversion mechanism. Our in situ experiments reveal direct evidence of the relationship between the lithium-storage behavior and performance of metal oxides in LIBs.

■ ASSOCIATED CONTENT

Supporting Information

The Supporting Information is available free of charge on the ACS Publications website at DOI: 10.1021/acsami.5b06548.

Ex situ TEM investigation of CuO electrodes in coin cells (PDF)

Lithiation of a CuO nanoparticle anchored on graphene nanosheet (AVI)

Lithiation of another CuO nanoparticle on graphene nanosheet (AVI)

■ AUTHOR INFORMATION

Corresponding Author

*E-mail: gaohuidu@zjnu.edu.cn.

Notes

The authors declare no competing financial interest.

■ ACKNOWLEDGMENTS

This work was supported by the National Science Foundation of China (Nos. 11574273, 11504330) and the Natural Science Foundation of Zhejiang Province (No. LQ15B010001).

■ REFERENCES

(1) Armand, M.; Tarascon, J. M. Building Better Batteries. *Nature* **2008**, *451*, 652−657.

(2) Wu, Z. S.; Zhou, G. M.; Yin, L. C.; Ren, W. C.; Li, F.; Cheng, H. M. Graphene/Metal Oxide Composite Electrode Materials for Energy Storage. *Nano Energy* **2012**, *1*, 107−131.

DOI: 10.1021/acsami.5b06548
ACS Appl. Mater. Interfaces 2015, 7, 23062−23068

(3) Yu, L.; Wu, H. B.; Lou, X. W. Mesoporous $Li_4Ti_5O_{12}$ Hollow Spheres with Enhanced Lithium Storage Capability. *Adv. Mater.* **2013**, *25*, 2296−2300.
(4) Jiang, J.; Li, Y.; Liu, J.; Huang, X.; Yuan, C.; Lou, X. W. Recent Advances in Metal Oxide-Based ElectrodeArchitecture Design for Electrochemical Energy Storage. *Adv. Mater.* **2012**, *24*, 5166−5180.
(5) Wang, H. W.; Xu, Z. J.; Yi, H.; Wei, H. G.; Guo, Z. H.; Wang, X. F. One-Step Preparation of Single-Crystalline Fe_2O_3 Particles/Graphene Composite Hydrogels as High Performance for Supercapacitors. *Nano Energy* **2014**, *7*, 86−96.
(6) Ding, S.; Chen, J. S.; Lou, X. W. One-Dimensional Hierarchical Structures Composed of Novel Metal Oxide Nanosheets on a Carbon Nanotube Backbone and Their Lithium-Storage Properties. *Adv. Funct. Mater.* **2011**, *21*, 4120−4125.
(7) Zhang, G.; Lou, X. W. Controlled Growth of $NiCo_2O_4$ Nanorods and Ultrathin Nanosheets on Carbon Nanofibers for High-Performance Supercapacitors. *Sci. Rep.* **2013**, *3*, 1470.
(8) Xu, Y.; Guo, J.; Wang, C. Sponge-Like Porous Carbon/Tin Composite Anode Materials for Lithium Ion Batteries. *J. Mater. Chem.* **2012**, *22*, 9562−9567.
(9) Su, D.; Kim, H. S.; Kim, W. S.; Wang, G. Mesoporous Nickel Oxide Nanowire: Hydrothermal Synthesis, Characterisation and Application for Lithium-Ion Batteries and Supercapacitors with Superior Performance. *Chem. - Eur. J.* **2012**, *18*, 8224−8229.
(10) Lou, X. W.; Archer, L. A.; Yang, Z. Hollow Micro-/Nanostructures: Synthesis and Applications. *Adv. Mater.* **2008**, *20*, 3987−4019.
(11) Wang, Z.; Zhou, L.; Lou, X. W. Metal Oxide Hollow Nanostructures for Lithium-Ion Batteries. *Adv. Mater.* **2012**, *24*, 1903−1911.
(12) Xu, S.; Hessel, C. M.; Ren, H.; Yu, R.; Jin, Q.; Yang, M.; Zhao, H.; Wang, D. α-Fe_2O_3 Multi-Shelled Hollow Microspheres for Lithium Ion Battery Anodes with Superior Capacity and Charge Retention. *Energy Environ. Sci.* **2014**, *7*, 632−637.
(13) Zhang, G.; Yu, L.; Wu, H. B.; Hoster, H. E.; Lou, X. W. Formation of $ZnMn_2O_4$ Ball-in-Ball Hollow Microspheres as a High Performance Anode for Lithium-Ion Batteries. *Adv. Mater.* **2012**, *24*, 4609−4613.
(14) Sahay, R.; Kumar, P. S.; Aravindan, V.; Sundaramurthy, J.; Ling, W. C.; Mhaisalkar, S. G.; Ramakrishna, S.; Madhavi, S. High Aspect Ration Electrospun CuO Nanofibers as Anode Material for Lithium-Ion Batteries with Superior Cycleability. *J. Phys. Chem. C* **2012**, *116*, 18087−18092.
(15) Zhou, X. Y.; Zhang, J.; Su, Q. M.; Shi, J. J.; Liu, Y.; Du, G. H. Nanoleaf-on-Sheet CuO/Graphene Composites: Microwave-Assisted Assemble and Excellent Electrochemical Performances for Lithium Ion Batteries. *Electrochim. Acta* **2014**, *125*, 615−621.
(16) Tarascon, J. M.; Poizot, P.; Laruelle, S.; Grugeon, S.; Dupont, L. Nano-Sized Transition-Metal Oxides as Negative-Electrode Materials for Lithium-Ion Batteries. *Nature* **2000**, *407*, 496−499.
(17) Wang, X.; Tang, D. M.; Li, H. Q.; Yi, W.; Zhai, T. Y.; Bando, Y.; Golberg, D. Revealing the Conversion Mechanism of CuO Nanowires during Lithiation-Delithiation by *In Situ* Transmission Electron Microscopy. *Chem. Commun.* **2012**, *48*, 4812−4814.
(18) Wang, C. M.; Xu, W.; Liu, J.; Choi, D.; Arey, B.; Saraf, L. V.; Zhang, J.; Yang, Z.; Thevuthasan, S.; Baer, D. R.; Salmon, N. *In Situ* Transmission Electron Microscopy and Spectorscopy Studies of Interfaces in Li Ion Batteries: Challenges and Opportunities. *J. Mater. Res.* **2010**, *25*, 1541−1547.
(19) McDowell, M. T.; Lee, S. W.; Harris, J. T.; Korgel, B. A.; Wang, C.; Nix, W. D.; Cui, Y. *In Situ* TEM of Two-Phase Lithiation of Amorphous Silicon Nanospheres. *Nano Lett.* **2013**, *13*, 758−764.
(20) Huang, J. Y.; Zhong, L.; Wang, C. M.; Sullivan, J. P.; Xu, W.; Zhang, L. Q.; Mao, S. X.; Hudak, N. S.; Liu, X. H.; Subramanian, A.; et al. *In Situ* Observation of the Electrochemical Lithiation of a Single SnO_2 Nanowire Electrode. *Science* **2010**, *330*, 1515−1520.
(21) Su, Q. M.; Xie, D.; Zhang, J.; Du, G. H.; Xu, B. S. *In Situ* Transmission Electron Microscopy Observation of the Conversion Mechanism of Fe_2O_3/Graphene Anode during Lithiation-Delithiation Processes. *ACS Nano* **2013**, *7*, 9115−9121.
(22) Su, Q. M.; Du, G. H.; Zhang, J.; Zhong, Y. J.; Xu, B. S.; Yang, Y.; Neupane, S.; Kadel, L.; Li, W. Z. *In Situ* Transmission Electron Microscopy Investigation of the Electrochemical Lithiation-Delithiation of the Individual Co_9S_8/Co-Filled Carbon Nanotubes. *ACS Nano* **2013**, *7*, 11379−11387.
(23) Wang, C. M.; Xu, W.; Liu, J.; Zhang, J. G.; Saraf, L. V. F.; Arey, B. W.; Choi, D.; Yang, Z. G.; Xiao, J.; Thevuthasan, S.; Baer, D. R. *In Situ* Transmission Electron Microscopy Observation of Microstructure and Phase Evolution in a SnO_2 Nanowire during Lithium Intercalation. *Nano Lett.* **2011**, *11*, 1874−1880.
(24) Wang, F.; Yu, H. C.; Chen, M. H.; Wu, L.; Pereira, N.; Thornton, K.; Van der Ven, A.; Zhu, Y.; Amatucci, G. G.; Graetz, J. Tracking Lithium Transport and Electrochemical Reactions in Nanoparticles. *Nat. Commun.* **2012**, *3*, 1201.
(25) Su, Q. M.; Zhang, J.; Wu, Y. S.; Du, G. H. Revealing the Electrochemical Conversion Mechanism of Porous Co_3O_4 Nanoplates in Lithium Ion Battery by *In Situ* Transmission Electron Microscopy. *Nano Energy* **2014**, *9*, 264−272.
(26) Su, Q. M.; Dong, Z. M.; Zhang, J.; Du, G. H.; Xu, B. S. Visualizing the Electrochemical Reaction of ZnO Nanoparticles with Lithium by *In Situ* TEM: Two Reaction Modes are Revealed. *Nanotechnology* **2013**, *24*, 255705.
(27) Hummers, W. S.; Offeman, R. E. Preparation of Graphitic Oxide. *J. Am. Chem. Soc.* **1958**, *80*, 1339.
(28) Ke, F. S.; Huang, L.; Wei, G. Z.; Xue, L. J.; Li, J. T.; Zhang, B.; Chen, S. R.; Fan, X. Y.; Sun, S. G. One-Step Fabrication of CuO Nanoribbons Array Electrode and Its Excellent Lithium Storage Performance. *Electrochim. Acta* **2009**, *54*, 5825−5829.
(29) Li, H.; Huang, X. J.; Chen, L. Q.; Zhou, G. W.; Zhang, Z.; Yu, D. P.; Mo, Y. J.; Pei, N. The Crystal Structural Evolution of Nano-Si Anode Caused by Lithium Insertion and Extraction at Room Temperature. *Solid State Ionics* **2000**, *135*, 181−191.
(30) Courtney, I. A.; McKinnon, W. R.; Dahn, J. R. On the Aggregation of Tin in SnO Composite Glasses Caused by the Reversible Reaction with Lithium. *J. Electrochem. Soc.* **1999**, *146*, 59−68.
(31) Larcher, D.; Masquelier, C.; Bonnin, D.; Chabre, Y.; Masson, V.; Leriche, J. B.; Tarascon, J. M. Effect of Particle Size on Lithium Intercalation into α-Fe_2O_3. *J. Electrochem. Soc.* **2003**, *150*, A133−A139.
(32) Wang, C.; Higgins, D.; Wang, F. F.; Li, D. Y.; Liu, R. Q.; Xia, G. F.; Li, N.; Li, Q.; Xu, H.; Wu, G. Controlled Synthesis of Micro/nanostructured CuO Anodes for Lithium-Ion Batteries. *Nano Energy* **2014**, *9*, 334−344.
(33) Li, A.; Song, H. H.; Wan, W. B.; Zhou, J. S.; Chen, X. H. Copper Oxide Nanowire Arrays Synthesized by *In-Situ* Thermal Oxidation as Anode Material for Lithium-Ion Batteries. *Electrochim. Acta* **2014**, *132*, 42−48.
(34) Wang, C.; Li, Q.; Wang, F. F.; Xia, G. F.; Liu, R. Q.; Li, D. Y.; Li, N.; Spendelow, J. S.; Wu, G. Morphology-Dependent Performance of CuO Anodes via Facile and Controllable Synthesis for Lithium-Ion Batteries. *ACS Appl. Mater. Interfaces* **2014**, *6*, 1243−1250.

DOI: 10.1021/acsami.5b06548
ACS Appl. Mater. Interfaces 2015, 7, 23062−23068